Electronic Supplementary Material (ESI) for Nanoscale.

Surface Charge Species and Electrochemical Dynamics on Ferroelectric Thin Film Surfaces - Supplementary Materials

Neus Domingo*

Catalan Institute of Nanoscience and Nanotechnology (ICN2), CSIC and BIST, Campus UAB, Bellaterra, 08193 Barcelona, Spain†

Iaroslav Gaponenko*

DQMP, University of Geneva, 1211, Geneva, Switzerland and G. W. Woodruff School of Mechanical Engineering, Georgia Institute of Technology, Atlanta, Georgia, USA‡

Kumara Cordero-Edwards

Catalan Institute of Nanoscience and Nanotechnology (ICN2), CSIC and BIST, Campus UAB, Bellaterra, 08193 Barcelona, Spain† *and DQMP, University of Geneva, 1211, Geneva, Switzerland*

Nicolas Stucki

University of Applied Sciences Western Switzerland in Geneva (HES-SO/hepia), 1213 Geneva, Switzerland

Virginia Pérez-Dieste and Carlos Escudero

ALBA Synchrotron Light Source, Carrer de la Llum 226, 08290 Cerdanyola del Vallès, Barcelona, Spain

Elzbieta Pach

Catalan Institute of Nanoscience and Nanotechnology (ICN2), CSIC and BIST, Campus UAB, Bellaterra, 08193 Barcelona, Spain† *and Institut de Ciència de Materials de Barcelona (ICMAB), CSIC, Campus UAB, Bellaterra, 08193 Barcelona, Spain*

Albert Verdaguer

Institut de Ciència de Materials de Barcelona (ICMAB),

CSIC, Campus UAB, Bellaterra, 08193 Barcelona, Spain

Patrycja Paruch

DQMP, University of Geneva, 1211, Geneva, Switzerland

* These authors contributed equally to this work.

† neus.domingo@icn2.cat

‡ iaroslav.gaponenko@unige.ch

I. FABRICATION AND STRUCTURAL CHARACTERISATION OF THE PZT THIN FILMS

The films were purchased from the University of Geneva spin-off Phasis, grown by N. Stucki of hepia, by off-axis radio frequency magnetron sputtering on conductive Nb-doped (0.5% weight) (001)-oriented single crystal SrTiO3 substrates heated to 510 C in 180 mTorr in an 10:20 oxygen:argon mixture, as detailed in reference [9]. The films were grown epitaxially on the substrate following the (001) orientation, so the polarisation axis is out of the plane of the film. The two films showed opposite polarisation as-grown, with one being monodomain up-polarised and the other down-polarised, as determined by writing reference structures of stripe domains with alternating positive and negative SPM tip voltage and imaging these together with the native, unswitched background using PFM.

XRD characterisation performed after the growth confirms the epitaxial (001) oriented growth. In theta-2theta scans, only the expected 00n peaks and no 110 peaks (corresponding to in-plane orientation of the polarisation axis in possible a-domains) were observed. Moreover, we observe no a-axis inclusions in either topographical or PFM images, thus suggesting that if there are a domains, they are sufficiently sparse to be below our detection limit. We note that in detailed measurements of the strain in PZT films 15 - 130 nm thick grown under the same conditions, full coherence with the substrate was reported up to a critical thickness of approximately 20 nm determined from fitting the c and a-axis parameter evolution, and subsequently the films begins to relax. This relaxation proceeds primarily by the formation of misfit dislocations, which create a short-range disorder in the crystal, as evidenced by the appearance of a broader diffuse scattering region around the rocking curve of the Bragg peak[3].

II. PATTERNING FERROELECTRIC DOMAINS IN THIN FILMS FOR AP-XPS EXPERIMENTS

The goal of the work is to compare the interaction of water and ferroelectric surfaces in areas with different polarization states. For the AP-XPS measurements, the patterning of the reversed polarization regions was carried out ex-situ on the down-polarized sample by using large area Au electrodes as shown in Fig. S1 to which - 10 V was applied to switch

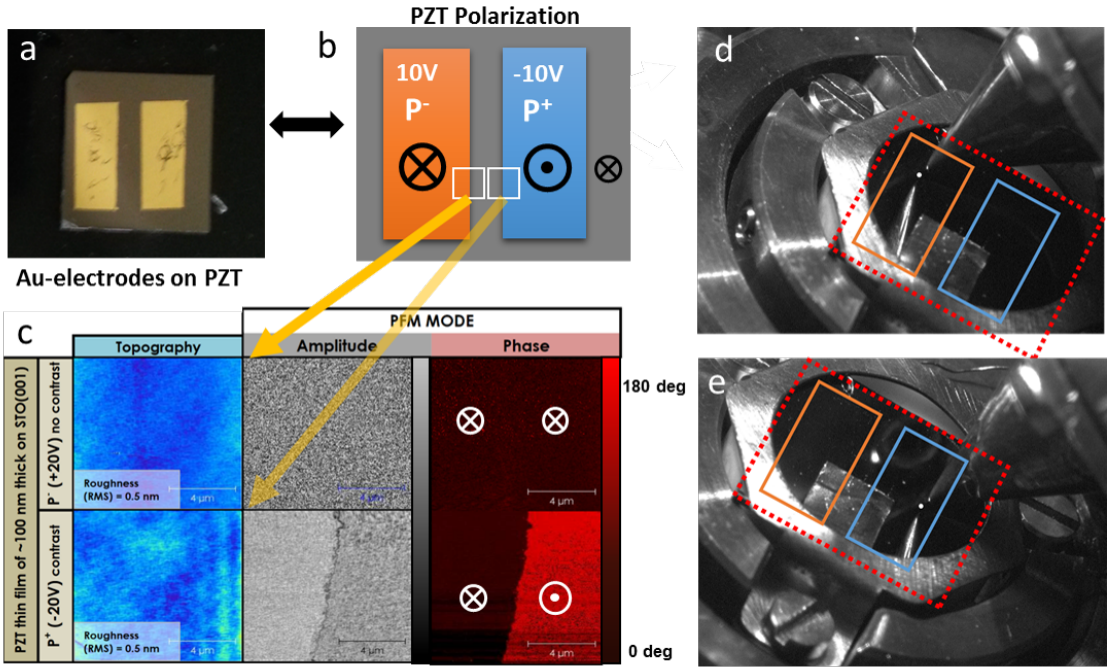

FIG. 1. (a) Optical image and (b) schematic representation of the PZT thin film with an as-grown down-polarized state with two gold electrodes deposited by evaporation and biased with - 10V (polarization switching). (c) Complete removal of gold electrodes was checked by topography and XPS, and the ferroelectric polarization state was checked by PFM. For the right electrode, a phase contrast of 180 deg is observed for the area below the removed electrode. (d) Optical image of the AP-XPS nose located on area 1 polarized up and (e) area 2 polarized down. The resolution of the camera allow a precise location of the analysis spot on the surface with enough precision to distinguish between the different areas where the electrodes were located

the polarization from the as-grown state. After switching, the electrodes were chemically removed by sonication in organic solvents and the surface topography and ferroelectric polarization of each area checked by SPM. Complete Au removal was further confirmed by XPS analysis on the electrode area. For the up-polarized sample, only the as-grown polarization state was measured.

III. DESCRIPTION OF THE XPS SPECTRA IN THE O1S REGION

The fitting of XPS spectra peaks was performed using the *CasaXPS* software with a combination of Gaussian/Lorentzian functions in the ratio of 70:30 after a Shirley subtraction,

except for the gas phase peak, where a 30:70 ratio was used. The lowest binding energy (BE) peak corresponding to bulk oxide was found at 530.5 eV, calibrated by taking the position of C1s C-C adventitious carbon as a reference. Five additional peaks were considered to fit the O1s region, four corresponding to surface adsorbates, as well as a fifth peak located at +(5.5±0.1)eV from the oxide peak, corresponding to the water gas phase (Fig. 3(a) in the main text). The four oxygen-related adsorbate peaks were positioned at ΔBE = +(1.0±0.1) eV, ΔBE = +(1.80.1) eV, ΔBE = +(2.6±0.2)eV and ΔBE = +(3.6±0.2)eV from the bulk oxide peak. The peak closest to the bulk oxide peak has been consistently related to the presence of hydroxyl groups in general. For the case of TiO_2 terminated surfaces, this peak can be associated with two types of hydroxyl groups: the terminal hydroxyl group (Ti-OH) and a bridging hydroxyl group (Ox-H)[4, 5, 7, 10], which can be considered as hydroxyl groups incorporated in the lattice[10] (hereafter named lattice OH). The peak at ΔBE≈1.8 eV from the oxide has been assigned to carbon oxide molecules (-COx)[12] or to carbonate species[1, 8]. Peaks located in the band between ΔBE≈2.4 eV and ΔBE≈3.6 eV from the oxide have been usually associated with adsorbed water on the surface either as molecular water or "pseudo-dissociated" water[5, 10] following a hydroxylation and protonation process (creating a pair of terminal and lattice -OH groups in a nearby position, possibly interacting through soft hydrogen bonds), followed by a back reaction to reform a water molecule with a small energy barrier of ≈0.4 eV between the two states[11]. However, recent studies of XPS on TiO_2 terminated surfaces extend the contribution to the lower part of this BE band to all types of chemisorbed oxygen species including those taking the form of peroxide groups[2, 6]. Here we associate the peak at ΔBE≈3.6 eV from the oxide to molecularly adsorbed water bound to other water molecules and the peak at ΔBE≈2.6 eV from the oxide to chemisorbed oxygen species from pseudo-dissociated water to peroxide groups (hereafter named the surface oxygen peak).

IV. SURFACE DISCHARGE DYNAMICS FROM AP-XPS

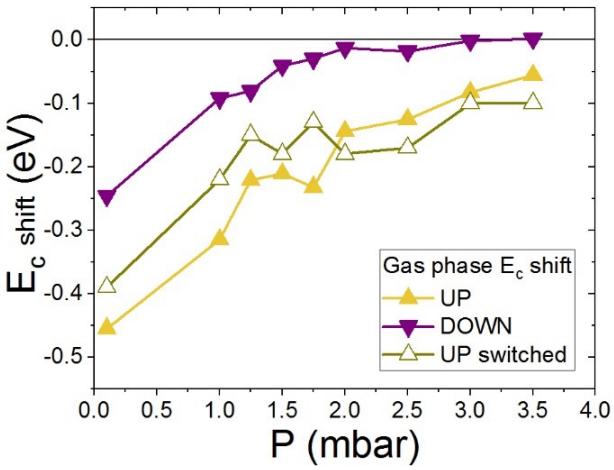

FIG. 2. Shift of the kinetic energy peak measured for the oxide peak contribution to the O1s spectral region with respect to the peak position at the highest RH. This energy shift is known to be sensitive to surface charge effects under XPS irradiation and stray fields.

V. SPATIAL CONFINEMENT OF THE KPFM SIGNAL

As shown in Fig. 1c and Fig. 1f of the main text, the observed KPFM signal has an increased spatial extent as humidity is increased. This extent is not only larger than that of the written domain area, but - crucially - it is established during the writing process and does not correspond to a gradual spread of surface charge once the biased tip is removed. While there is an evident decrease of the surface potential intensity over time, the KPFM signal remains confined to the initial boundaries. This is illustrated in Fig. S3, where the spatial cross-sectional average of the KPFM signal is shown as a function of time for two representative relative humidities for the as-grown down-polarized sample. The initial KPFM images after writing are shown in Fig. S3(a) and (d), for 26% and 61% relative humidity respectively. The outlined rectangles shown in the KPFM images are used to extract averages along the short spatial axis, giving an average KPFM cross-section for each image in a series of 30. Tthe resulting normalized time average and its absolute derivative is shown in Fig. S3(b,c) and in Fig. S3(e,f) for the two humidities, respectively. No spatial spread is observed in either of these signals. We can therefore conclude that the KPFM signal is based on fixed surface charges, rather than mobile diffusive charge species.

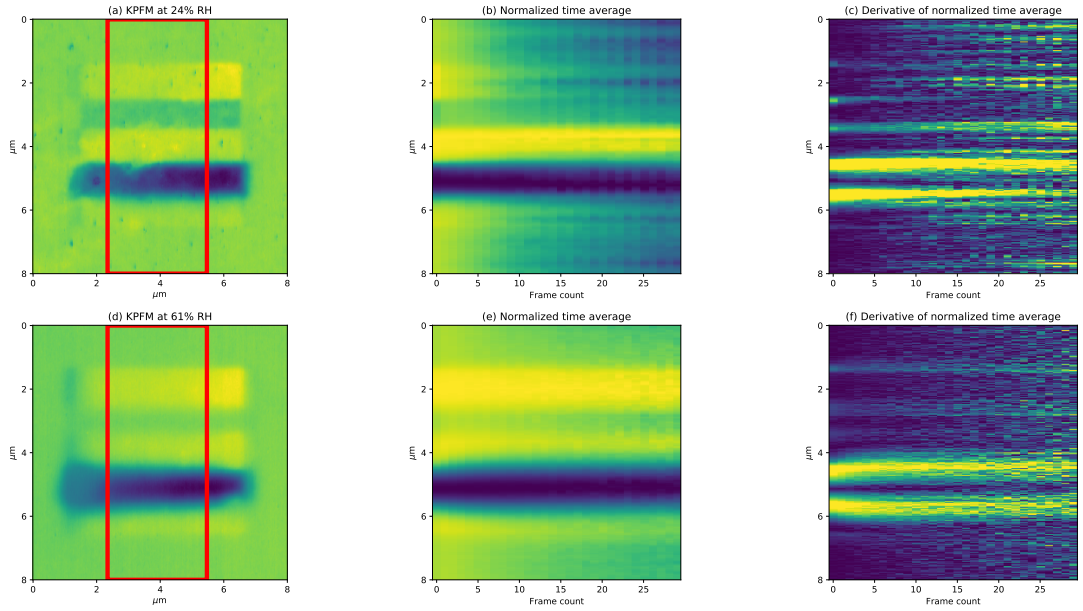

FIG. 3. Time evolution of the KPFM signal for 26% and 61% relative humidity in the down-polarized as-grown sample. The initial KPFM images (a) and (d) for the two humidities are averaged along the short axis of the red rectangle. The process is repeated for a series of 30 images and yields the normalized time evolution of the average KPFM signal cross-section in (b) and (e). The absolute derivative of this average in (c) and (f) shows no time-dependent spatial spread of the KPFM signal.

VI. FITTING OF TIME DECAY OF KPFM SIGNAL

Figure S4 shows the relaxation of the KPFM signal over time.

The fits were constrained and optimized together for each applied voltage with a coupled time constant τ_{fast} (Fig. S5(a))for the fast sample-dependent decay which has a polarity-dependent intensity A_{fast1} or A_{fast2} (Fig. S5(b)). With these constraints, the fit performed simultaneously on all the data sets of surface potential decay for both positive and negative applied voltages as a function of humidity yielded excellent agreement, and a distribution of charge decay time constants. The τ_{fast} exponent shown in Fig. S5(a) was found to be largely independent of humidity. This lack of humidity dependence indicates that once the water layer is formed (for RH > 10 %), this fast process is a material-characteristic behavior which does not depend on the environment in which the sample is placed. As a first approach, and in agreement with the discharge process observed by XPS (see Fig. S2) we correlate

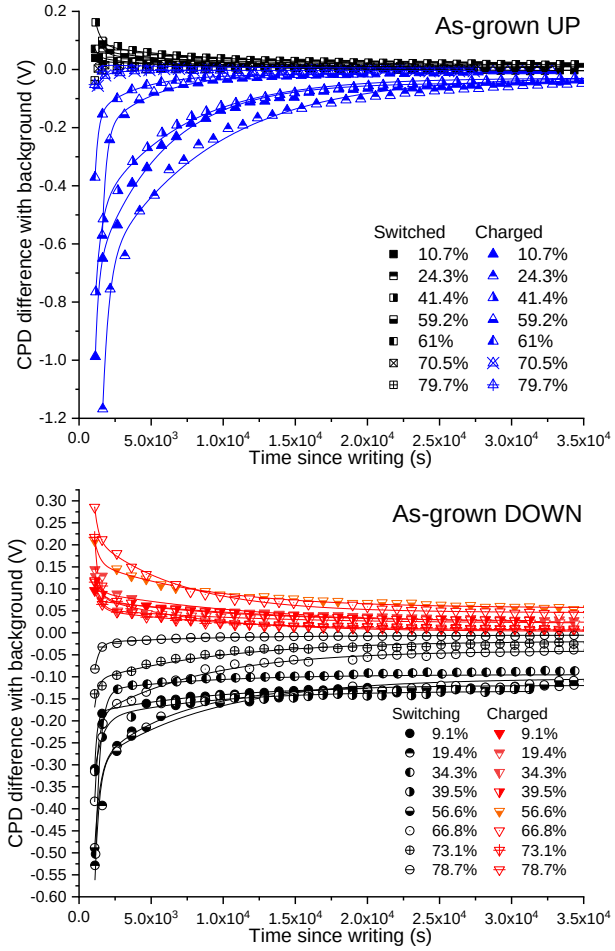

FIG. 4. KPFM contrast as a function of time for a) as-grown UP and b) as-grown DOWN samples

these dynamics to the water-mediated surface-conductivity based discharge of free charges, though some minor discharge through bulk electronic conductivity cannot be excluded.

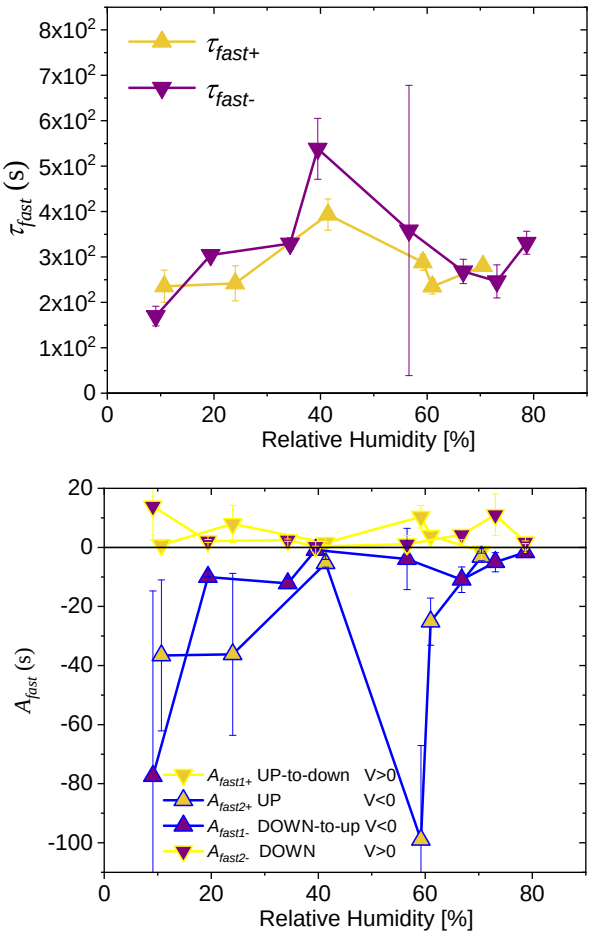

FIG. 5. Fitting parameters for the fast relaxation component of equation 1 a) coupled time constant τ_{fast} and b) polarity-dependent intensity for the fast decay A_{fast1} or A_{fast2}

VII. COMPARISON BETWEEN THE KPFM AND PFM SIGNALS

Successful polarization reversal and the exact shape of the switched, charged and contact-scanned regions was confirmed by PFM imaging in the down-polarized as-grown sample at different RH, and compared to the spatial extent of the KPFM signal. We note that the two measurements could not be carried out on the same SPM-patterned domain structure, as PFM imaging is a contact technique, and carrying it out directly after writing significantly changes the surface potential. KPFM, in contrast, is a resonant non-contact technique which was used to non-perturbatively probe the surface potential and its evolution directly after domain writing. Thus, identical domain structures were written with the identical protocol under the same RH conditions, and then one structure was imaged by PFM, and the other

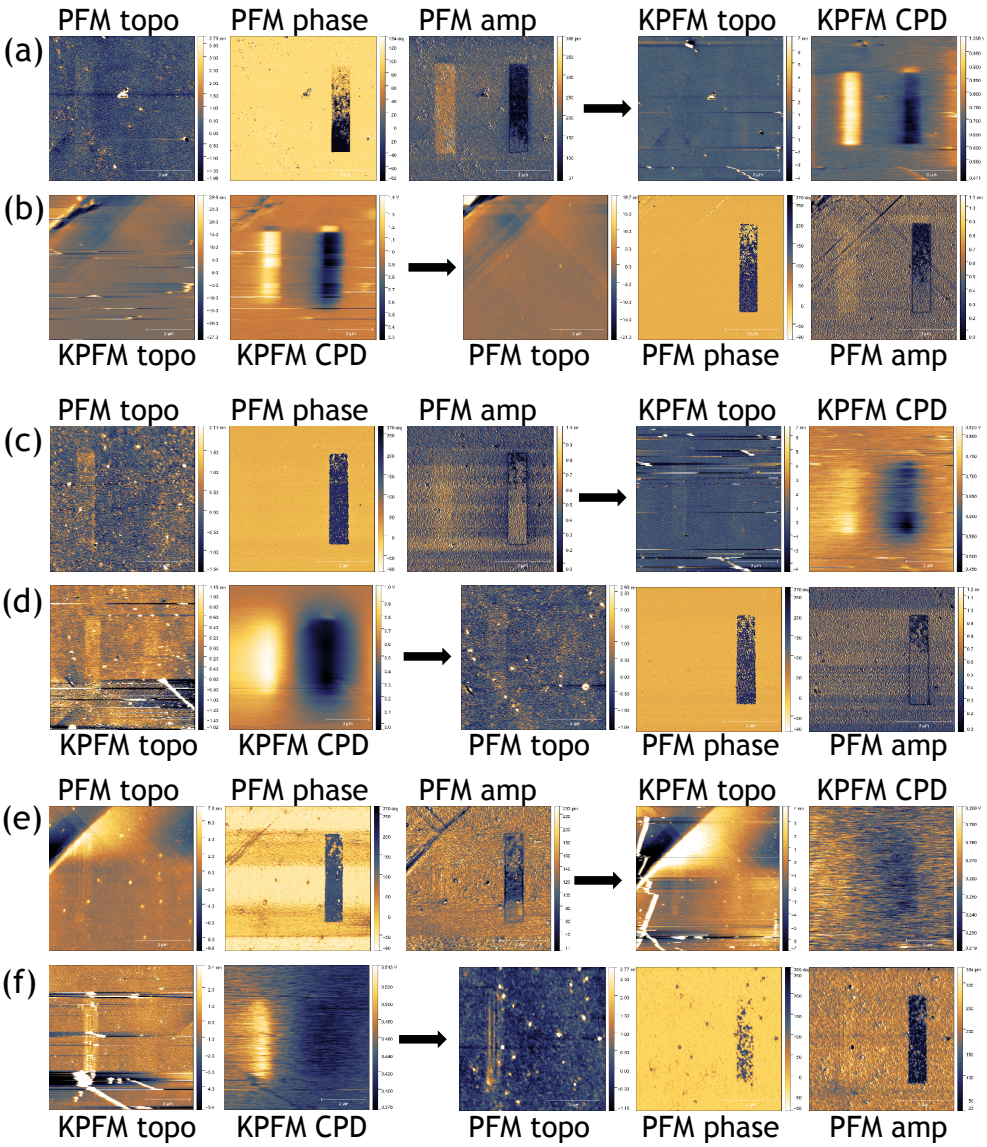

FIG. 6. PFM/KPFM and KPFM/PFM sequences performed at (a,b) 7% RH, (c,d) 40% RH, and (e,f) 70% RH on the as-grown down-polarized sample. Each sequence was preceded by the bias writing of the domain structure, and followed by a series of PFM or KPFM images. After one to two hours of imaging, KPFM or PFM was respectively performed to assess the evolution and spatial spread of the signal.

by KPFM. As can be seen in Fig. S6 for low (7%), medium (40%) and high (70%) RH, the ferroelectric domains themselves are contained within the perfectly rectangular region of writing, following the spatial pattern imposed by the biased scanning SPM tip, and the PFM phase signal does not show observable evolution with time. In contrast, the KPFM signal

is limited to the domain area itself at low RH, but extends well beyond the corresponding domain boundaries at higher RH.

---

[1] J. D. Baniecki, M. Ishii, K. Kurihara, K. Yamanaka, T. Yano, K. Shinozaki, T. Imada, and Y. Kobayashi. Chemisorption of water and carbon dioxide on nanostructured BaTiO3-SrTiO3(001) surfaces. *Journal of Applied Physics*, 106(5), SEP 1 2009. ISSN 0021-8979. doi:10.1063/1.3169654.

[2] Y. Gao, Y. Masuda, and K. Koumoto. Light-excited superhydrophilicity of amorphous TiO2 thin films deposited in an aqueous peroxotitanate solution. *Langmuir*, 20(8):3188–3194, APR 13 2004. ISSN 0743-7463. doi:10.1021/la0303207.

[3] S. Gariglio, N. Stucki, and J.-M. Triscone. Strain relaxation and critical temperature in epitaxial ferroelectric pb($zr_{0.20}ti_{0.80}$)o_3 thin films. *Applied Physics Letters*, 90:202905, 2007.

[4] M. J. Jackman, A. G. Thomas, and C. Muryn. Photoelectron Spectroscopy Study of Stoichiometric and Reduced Anatase TiO2(101) Surfaces: The Effect of Subsurface Defects on Water Adsorption at Near-Ambient Pressures. *Journal of Physical Chemistry C*, 119(24): 13682–13690, JUN 18 2015. ISSN 1932-7447. doi:10.1021/acs.jpcc.5b02732.

[5] G. Ketteler, S. Yamamoto, H. Bluhm, K. Andersson, D. E. Starr, D. F. Ogletree, H. Ogasawara, A. Nilsson, and M. Salmeron. The nature of water nucleation sites on TiO2(110) surfaces revealed by ambient pressure X-ray photoelectron spectroscopy. *Journal of Physical Chemistry C*, 111(23):8278–8282, JUN 14 2007. ISSN 1932-7447. doi:10.1021/jp068606i.

[6] I. Krivtsov, M. Ilkaeva, E. Salas-Colera, Z. Anighouz, J. R. Garcia, E. Diaz, S. Ordonez, and S. Villar-Rodil. Consequences of Nitrogen Doping and Oxygen Enrichment on Titanium Local Order and Photocatalytic Performance of TiO2 Anatase. *Journal of Physical Chemistry C*, 121(12):6770–6780, MAR 30 2017. ISSN 1932-7447. doi:10.1021/acs.jpcc.7b00354.

[7] W. Li, S. Liu, S. Wang, Q. L. Guo, and J. Guo. The Roles of Reduced Ti Cations and Oxygen Vacancies in Water Adsorption and Dissociation on SrTiO3(110). *Journal of Physical Chemistry C*, 118(5):2469–2474, FEB 6 2014. ISSN 1932-7447. doi:10.1021/jp409076y.

[8] A. Song, E. S. Skibinski, W. J. I. DeBenedetti, A. G. Ortoll-Bloch, and M. A. Hines. Nanoscale Solvation Leads to Spontaneous Formation of a Bicarbonate Monolayer on Rutile (110) under Ambient Conditions: Implications for CO2 Photoreduction. *Journal of Physical Chemistry*

C, 120(17):9326–9333, MAY 5 2016. ISSN 1932-7447. doi:10.1021/acs.jpcc.6b02132.

[9] N. Stucki. *Artificial ferroelectric materials*. PhD thesis, Universit de Genve, urn:nbn:ch:unige-5311, 2 2008. An optional note.

[10] J. L. Wang, F. Gaillard, A. Pancotti, B. Gautier, G. Niu, B. Vilquin, V. Pillard, G. L. M. P. Rodrigues, and N. Barrett. Chemistry and Atomic Distortion at the Surface of an Epitaxial BaTiO3 Thin Film after Dissociative Adsorption of Water. *Journal of Physical Chemistry C*, 116(41):21802–21809, OCT 18 2012. ISSN 1932-7447. doi:10.1021/jp305826e.

[11] S. Wendt, J. Matthiesen, R. Schaub, E. Vestergaard, E. Laegsgaard, F. Besenbacher, and B. Hammer. Formation and splitting of paired hydroxyl groups on reduced TiO2(110). *Physical Review Letters*, 96(6), FEB 17 2006. ISSN 0031-9007. doi:10.1103/PhysRevLett.96.066107.

[12] Y. Zhang, A. Savara, and D. R. Mullins. Ambient-Pressure XPS Studies of Reactions of Alcohols on SrTiO3(100). *Journal of Physical Chemistry C*, 121(42):23436–23445, OCT 26 2017. ISSN 1932-7447. doi:10.1021/acs.jpcc.7b06319.